Desalination and Water Treatment
www.deswater.com

doi: 10.5004/dwt.2020.26429

207 (2020) 270–286
December

Optimizing and modeling Cu(II) removal from simulated wastewater using attapulgite modified with Keggin ions with the aid of RSM, BP-ANN, and GA-BP

Weifang Xie[a], Ting Cheng[a], Chen Chen[b,*], Chao Sun[c,*], Lin Qi[a], Zhenming Zhang[d]

[a]*School of Environment and Ecology, Jiangsu Open University, Nanjing, Jiangsu 210036, China, emails: xiewf@jsou.cn (W. Xie), 327368287@qq.com (T. Cheng), 15846448@qq.com(L. Qi)*
[b]*School of Environmental and Chemical Engineering, Jiangsu University of Science and Technology, Zhenjiang 212003, China, email: chenc@just.edu.cn (C. Chen)*
[c]*The Key Laboratory of Chemistry for Natural Products of Guizhou Province and Chinese Academy of Sciences, Guiyang 550002, China, email: chaosun2000@hotmain.com (C. Sun)*
[d]*Guizhou Institute of Biology, Guiyang, Guizhou 550009, China, email: 417509234@qq.com (Z. Zhang)*

Received 17 February 2020; Accepted 3 August 2020

ABSTRACT

Attapulgite modified with Keggin ions was successfully synthesized to remove Cu(II) in aqueous systems. The original and modified attapulgite samples were characterized by X-ray diffraction, Fourier transform infrared spectroscopy, scanning electron microscopy, and X-ray photoelectron spectroscopy, and the adsorption capacity for Cu(II) of both materials was compared in this study. The parameters, such as contact time, initial pH, temperature, and initial Cu(II) concentration, affecting the adsorption efficiency of Cu(II) on the modified composite were evaluated using analysis of variance, aggregated boosted tree analysis, and random forest analysis. To obtain the maximum efficiency of Cu(II) removal from simulated wastewater, response surface methodology, a back propagation artificial neural network, and a genetic algorithm combined with a back propagation neural network (GA-BP) were utilized to optimize the operating parameters (temperature, contact time, initial pH, and initial Cu(II) concentration). The results showed that initial pH was the most influential variable for Cu(II) removal from aqueous solutions. GA-BP was the most suitable approach for modeling Cu(II) removal from aqueous solutions because its absolute error between the experimental and predicted values was the smallest. For GA-BP optimization, the maximum removal efficiency of Cu(II) reached 91.35% at temperature = 29.73°C, contact time = 69.60 min, initial pH = 6.46, and initial Cu(II) concentration = 100.00 mg/L. The results of adsorption isotherm, kinetics, and thermodynamics analysis showed that the Langmuir isotherm and pseudo-second-order kinetic model could describe the adsorption process, which was a spontaneous and entropy-driven process. The regeneration experiments showed that the attapulgite modified with Keggin ions for Cu(II) removal from simulated wastewater are an effective and reusable adsorbent within four regeneration cycles.

Keywords: Attapulgite; Keggin ion; Response surface methodology; Back propagation artificial neural network; Genetic algorithm combined with back propagation neural network

* Corresponding authors.

1. Introduction

Copper (Cu) is an essential element for humans and plants, and there are several materials containing various forms of copper compounds in the human living environment [1,2]. The amount of Cu emissions is increasing, leading to excessive Cu concentrations in plants, which will insignificantly damage human health and destroy the ecological environment through food chain enrichment [3]. The toxicity of divalent copper is greater than that of copper, especially $Cu(COOH)_2$ and Cu_2SO_4 [4]. Symptoms such as abdominal pain, diarrhea, and vomiting will emerge when excessive Cu is ingested by mistake [5]. Therefore, it is urgent to treat high concentrations of Cu(II) in wastewater.

Attapulgite ($Mg_5Si_8O_{20}(OH)_2(OH_2)_4{\cdot}4H_2O$) has a large specific surface area and high surface activity [6]. However, its application in environmental remediation is limited due to a large amount of hydroxyl groups on its surface and its easy agglomeration. Thus, it is necessary to modify attapulgite using several methods. Feng et al. [7] reported that porous attapulgite (ATP)/polymer beads were used to remove Cu(II) and Cd(II) from aqueous solutions, and the maximum adsorption capacities of the beads for Cu(II) and Cd(II) were 25.3 and 32.7 mg/g, respectively. Additionally, the beads were millimeter-sized and could float on the water surface, making such beads easy to handle and facile to recover without loss of mass. Falayi and Ntuli [8] utilized attapulgite calcined at 973.15 K as an adsorbent for the removal of heavy metals. After 2 h, the removal rates of Cu(II), Fe(II), Co(II), Ni(II), and Mn(II) were 100%, 99.46%, 96.20%, 86.92%, and 71.52%, respectively, using a loading of 2.50% w/v activated attapulgite. Zheng et al. [9] described that polyacrylic acid/attapulgite (PAA/ATP) composite hydrogels were used for the removal of heavy metal ions from aqueous solution. The results showed that the composite hydrogels had a large adsorption capacity for Ni(II) ions, and the average adsorption capacity reached 72.8 mg/g. Furthermore, Keggin ions have a high-charge polymerized ring shape, a high degree of neutralization and a strong bridging effect on colloids and particles in water and are suitable for the removal of micro poisons and heavy metal ions [10]. To date, Keggin ion-modified attapulgite has been rarely reported. Therefore, Keggin ion-modified attapulgite will be further investigated in this study based on previous works.

The operating conditions of the removal process greatly influence the removal efficiency. To obtain the maximum removal efficiency, response surface methodology (RSM) [11], back propagation artificial neural networks (BP-ANN) [12,13], and back propagation-genetic algorithm (BP-GA) neural networks [14,15] have been used to optimize the removal conditions. Hazime et al. [16] reported that the optimization of the photocatalytic degradation of a carcinogenic pesticide, imazalil, was carried out in an aqueous solution using TiO_2 as a photocatalyst under UV irradiation in the presence of persulfate. The optimal experimental conditions found for imazalil (25 mg/L) removal were an acidic pH of 3–4, persulfate concentration of ≈2.5 g/L, and TiO_2 loading of 2.5 g/L. The experimental design allows obtaining the maximum efficiency with the minimum amount of persulfate. This study systematically demonstrates the utility and benefits of the experimental design approach for screening and modeling reaction parameters. Liu et al. [17] created a back propagation (BP) neural-network model to estimate chlorophyll concentrations in rice under heavy metal stress. The results showed that the optimum BP neural-network prediction model had a 4-10-2-1 network architecture with a gradient descent learning algorithm and an activation function including a sigmoid tangent function in the input layer, a hidden layer and sigmoid logistic functions in the output layer. Awad et al. [18] investigated the capability of a real genetic algorithm to remove a heavy metal pollutant plume from an aquifer. A new system was developed for removing Hg and Cd from groundwater in a real problem and was proven to be optimal. The results showed that real-coding genetic algorithms are a practical means of optimizing engineering solutions to problems related to groundwater quality management, particularly those involving discontinuous functions. Nevertheless, the performance of ANNs should still be significantly improved due to the ease of falling into a local optimum. To avoid this problem, an ANN combined with a genetic algorithm (GA) will be used in this study.

Analysis of variance (RSM), random forest (RF) analysis, and aggregated boosted tree (APT) analysis can be used to evaluate the importance of factors, which has commonly been ignored in previous studies [19,20]. In contrast with previous reports, this study is devoted to applying artificial intelligence tools (BP-ANN, GA-BP, RF, and APT) in environmental remediation (Cu(II) removal from simulation wastewater). Generally, the purposes of this study were to (1) remove Cu(II) from aqueous solution using Keggin ion-modified attapulgite; (2) investigate the mechanism of the removal process through isothermal adsorption, kinetics, and thermodynamic parameters; (3) optimize the removal parameters to obtain the maximum Cu(II) removal efficiency by using RSM, a BP-ANNand BP-GA; and (4) evaluate the factor importance using RF (R language), the ABT gbmplus package (R language) and analysis of variance (RSM).

2. Materials and methods

2.1. Materials

The $A1Cl_3$ and NaOH used in this study were of analytical grade, and all solutions were prepared using deionized water. Attapulgite was obtained from Xuyi, (Jiangsu, China). Cu(II) stock solution (1,000 mg/L) was prepared by dissolving a known amount of $CuSO_4{\cdot}5H_2O$ in deionized water.

2.2. Preparation of Keggin ions

First, 0.2 mol/L $A1Cl_3$ and 0.5 mol/L NaOH solutions were prepared. Then, a certain amount of $A1Cl_3$ solution was put in a beaker, and the solution was heated and rapidly stirred in a constant temperature water bath at 60°C. NaOH solution was gradually dropped into the $A1Cl_3$ solution according to the ratio OH^-/Al^{3+} = 2.4 mol. The mixtures were transferred into a conical flask and then continuously stirred and heated for 2 h. After the end of stirring and

heating, the mouth of the flask was sealed with a rubber plug. Finally, colorless and transparent Keggin ion solutions were obtained after aging at 60°C for 2 d.

2.3. Preparation of Keggin ion-modified attapulgite

The purified attapulgite was weighed according to the ratio Al^{3+}/attapulgite = 5 mmol/g. The weighed attapulgite was added to Keggin ion solutions under continuous stirring and heating (the temperature was controlled at 80°C). Mixing was stopped after 2 h, the bottle mouth was plugged, and the mixture was left at 80°C for 48 h. The upper clear liquid was removed, and the flocculent precipitate was repeatedly washed with distilled water and filtered until the pH value of the filtrate was neutral. After natural drying, the filter cake was put in a constant temperature drying oven and dried at 105°C for 2 h to obtain Keggin ion-modified attapulgite.

2.4. Characterization of as-prepared Keggin ion-modified attapulgite

The Keggin ion-modified attapulgite was examined on X-ray diffraction (XRD) instrument for phase identification using a LynxEye array detector with a Cu-Kα X-ray source (accelerating voltage = 40 kV, current 40 mA, Bruker Corporation, Karlsruhe, Germany). The morphology was examined using TEM (TecnaiG2 F20, FEI Co., Ltd., Hillsboro, OR, USA). XPS measurements were recorded on an ESCALAB 250Xi spectrometer using monochromatized Al-Kα radiation (hν = 1,486.6 eV), and all binding energies were calibrated by using the contaminant carbon peak (C1S = 284.8 eV) as a reference (Thermo Electron Corporation, Waltham, MA, USA). FTIR measurements were performed using a Nicolet 6700 spectrometer (Nicolet Instrument Corporation, Madison, WI, USA). Magnetization measurements were carried out using a SQUID magnetometer (MPMS XL-7, Quantum Design, Inc., San Diego, CA, USA) under an applied magnetic field at room temperature. Brunner–Emmet–Teller (BET) surface areas of the Keggin ion-modified attapulgite were obtained from N_2 adsorption isotherms at 77 K with a Micromeritics 3 Flex surface characterization analyzer (outgas time: 3.0 h, outgas temperature: 300.0°C, Micromeritics Instrument Corporation, Norcross, GA, USA). Excel, Origin 8.6, and RSM (2011) were used for statistical data analysis, drawing, and experimental design, respectively. Random forest and integrated boosted tree analyses were carried out using the "random forest" and "gbmplus" packages in R2.9.2 software, respectively.

2.5. Adsorption experiments

The prepared 1,000 mg/L Cu(II) stock solution was gradually diluted to 100, 150, and 200 mg/L. Modified attapulgite (0.5 g) was added to 50 mL of Sb(III) solution (100, 150, and 200 mg/L). The initial pH of the mixture was adjusted to the desired value by using 0.1 mol/L HCl or 0.1 mol/L NaOH. The factors, including initial Cu(II) concentration, initial pH, contact time, and operating temperature, affecting the removal efficiency of Cu(II) were investigated using batch adsorption experiments (single-factor experiments). The Cu(II) concentration of the sample solutions was determined using inductively coupled plasma optical emission spectrometry (Optima 5300 V). From among all experiments, 20% were randomly selected for replication, and the average values of the results were used for data analysis. For each heavy metal, the accuracy and precision of the methods and results were checked by using the certified Standard Reference Material (GNM-M17270-2013), which was purchased by the Guobiao (Beijing) Testing and Certification Co., Ltd.

The removal efficiency of Cu(II) from stock solution using modified attapulgite was calculated from Eq. (1):

$$P = \frac{\left(C_0 - C_t\right) \times 100}{C_0} \tag{1}$$

where P is the removal efficiency of Cu(II), C_t is the Cu(II) concentration after removal, and C_0 is the initial Cu(II) concentration (mg/L).

The Cu(II) adsorption quantity was calculated by Eq. (2):

$$q_e = \frac{\left(C_0 - C_t\right) \times v}{m} \tag{2}$$

where q_e is the quantity of Cu(II) adsorbed on the modified attapulgite at equilibrium (mg/g); C_0 and C_t are the initial and equilibrium Cu(II) concentrations (mg/L), respectively; v is the volume (L) of the solution; and m is the adsorbent mass (g).

2.6. RSM used for experimental design

In order to reduce the number of experiments, a Box–Behnken design (BBD) approach of RSM was used in this study. The interaction effect of four factors was analyzed by a 4-factor-5-level BBD, and the process parameters were optimized, that is, contact time (*A*), initial Cu(II) concentration (*B*), temperature (*C*), and initial pH (*D*). The BBD design consists of two cube points (1 and +1) and a center point (0). Each variable changes at three levels (–1, 0, and +1), and a second-order model (Eq. (3)) was established to evaluate the impact of process parameters [21].

$$Y = \beta_0 + \sum_{i=1}^{k} \beta_i x_i + \sum_{i=1}^{k} \beta_{ii} \left(x_i\right)^2 + \sum_{i=1}^{k-1} \sum_{j=2}^{k} \beta_{ij} x_i x_j \tag{3}$$

where Y is the calculated response associated with each factor level combination; β_0, β_i, β_{ii}, and β_{ij} are the regression parameters (β_0 is the intercept, β_i is the linear effect term, β_{ii} is the square effect term and β_{ij} is the interactive effect term); x_i and x_j are the coded levels of independent variables; and the terms $x_i x_j$ and $(x_i)^2$ (i = 1 to k and j = 2 to k) represent the interaction and quadratic terms, respectively. The range of each factor is determined by a single-factor experiment, the results of which are shown in Table 1. According to the experimental design, 29 sets of conditions needed to be carried out in this study, among which the data from 24 data sets were used for modeling, and the remaining five data sets were used to verify the model.

2.7. GA-BP used for optimizing parameters

BP neural networks are a kind of multilayer feedforward neural network (Fig. 1). The main characteristics of these networks are signal forward transmission and error back propagation [22]. In the process of forward propagation, the input signal is processed from the input layer to the output layer through the hidden layer [23,24]. The state of neurons in each layer only affects the state of neurons in the next layer. If the output layer cannot produce the expected output, back propagation will occur, and the network weight and threshold will be adjusted according to the prediction error so that the predicted output of the BP neural network will keep approaching the expected output.

In the process of network initialization, according to the input and output sequence of the system, the number of network input layer nodes, the number of hidden layer nodes, the number of output layer nodes, the sum of the connection weights between the input layer, the hidden layer, and the output layer neurons, the threshold a of the hidden layer and the threshold of the output layer are initialized, and the learning rate and the neuron excitation function are given. In the second step, according to the input variable x, the connection weight w_{ij} of the input layer and hidden layer, and the hidden layer threshold a, afterwards, the hidden layer output H is calculated.

$$H_i = f\left(\sum_{i=1}^{n} x_{ij}x_i - a_j\right) \qquad j = 1,2,3,\ldots,l \tag{4}$$

where l is the number of nodes in the hidden layer and f is the excitation function of the hidden layer. A sigmoid function was employed in this study.

$$f(x) = \frac{1}{1+e^{-x}} \tag{5}$$

In the third step, according to the output H of the hidden layer, the connection weight w_{jk}, and threshold b, the output O of the BP neural network is calculated.

$$O_k = \sum_{j=1}^{i} H_j w_{jk} - b_k \qquad k = 1,2,3,\ldots,m \tag{6}$$

where m is the output layer node number.

For the fourth step, the prediction error e is calculated according to the prediction output O and the expected output y.

$$e_k = Y_k - O_k \qquad k = 1,2,3,\ldots,m \tag{7}$$

In the fifth step, the network connection weights of w_{ij} and w_{jk} are updated according to the network prediction error E.

$$w_{ij} = w_{ij} + vH_j\left(1-H_j\right)\times(i)\sum_{k=1}^{m} w_{jk}e_k \qquad i = 1,\ 2,\ 3,\ ...,\ l;\quad k = 1,\ 2,\ 3,\ ...,\ m \tag{8}$$

$$w_{jk} = w_{jk} + vH_j e_k \qquad j = 1,\ 2,\ 3,\ ...,\ l; \qquad k = 1,\ 2,\ 3,\ ...,\ m \tag{9}$$

where v is the learning rate.

In the sixth step, the node thresholds a and b are updated according to the network prediction error e.

$$a_j = q_j + vH_j\left(1-H_j\right)\sum_{k=1}^{m} w_{ik}e_k \qquad j = 1,\ 2,\ 3,...,\ l \tag{10}$$

$$b_k = b_k + e_k \qquad k = 1,\ 2,\ 3,\ ...,\ m \tag{11}$$

Table 1
Level of parameters in Box–Behnken experimental design

Code	Parameters	Maximum values	Middle values	Minimum values
A	Contact time (min)	70	60	50
B	Initial Cd(II) concentration (mg/L)	30	20	10
C	Temperature (°C)	30	25	20
D	Initial pH values	7	6	5

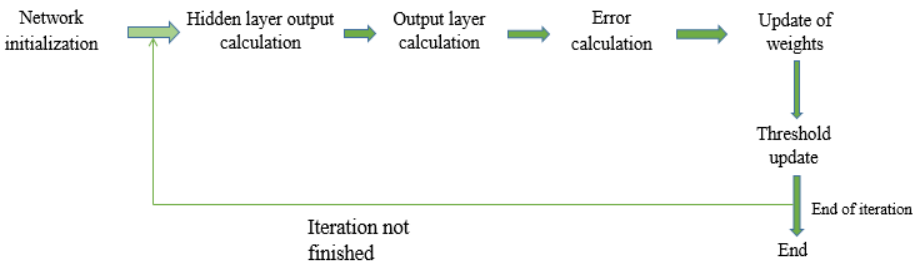

Fig. 1. BP network operation diagram.

The genetic algorithm (GA) approach is a parallel random search optimization method that simulates the genetic mechanism of nature and the theory of biological evolution (Fig. 2) [25]. Individuals with good fitness values are retained, and individuals with poor fitness are evaluated according to the selected fitness function and through selection, crossover, and mutation in genetics [26]. The new population not only inherits the information of the previous generation but also exceeds the previous generation. Three parts of the BP network, that is, neural network structure determination, genetic algorithm optimization, and BP neural network prediction, are optimized by the genetic algorithm [27]. Among these steps, the genetic algorithm was used to optimize the initial weight and threshold of the BP neural network, rendering the optimized BP neural network better able to predict the function output. The objective of the genetic algorithm in optimizing a BP neural network is to obtain better initial weights and thresholds. Generally, the main idea is to use an individual value to represent the initial weights and thresholds of the network, use the prediction error of the BP neural network initialized with the individual value as the fitness value of the individual value, and find the optimal individual value through selection, crossover and mutation operations, that is, the optimal initial BP neural network weights in this study. where N is the number of output nodes of the network; Y_i is the expected output of the ith node of the BP neural network; O_i is the actual output of the ith node; k is the coefficient; F_i is the fitness value of individual i; n is the number of individuals in the population; b is a random number between 0 and 1; a_{max} is the upper bound of a_{ij}; and a_{min} is the lower bound of a_{ij}.

3. Results and discussion

3.1. Characterization of attapulgite modified with Keggin ions

As shown in Fig. 3, the characteristic diffraction peaks of attapulgite are at 2θ = 8.65°, 26.91°, and 34.87° [28]. The characteristic diffraction peaks of SiO_2 are found at 2θ = 19.99° and 20.83° [29]. The characteristic peaks at 31.19° and 66.62° are attributed to Al_2O_3 [30]. In addition, quartz and montmorillonite impurities associated with attapulgite are found. The strongest peak at 26.91° is the characteristic diffraction peak of quartz [31], and the diffraction peaks of montmorillonite are located at 50.39° and 61.94° [32]. The diffraction peaks of quartz and montmorillonite in the modified attapulgite obviously decreased in comparison with those of attapulgite before modification using Keggin ions. This decrease showed that some impurities in the original attapulgite material can be separated by Keggin ion modification. Moreover, XRD analysis showed that the structure of attapulgite did not change significantly after Keggin ion modification.

An obvious absorption peak of pure attapulgite is found at approximately 3,500 cm^{-1} (Fig. 4), which is the absorption peak of different hydroxyl stretching vibrations in the attapulgite structure. The absorption peak at 1,656 cm^{-1} is attributed to the bending vibration absorption of carbonyl groups. The absorption peak at 1,197 cm^{-1} may be caused by the stretching vibration of (Mg, Al)–O bonds. The absorption band at 1,027 cm^{-1} may be caused by the stretching vibration of Si–O bonds, and the absorption peak at 982 cm^{-1} may be attributed to the stretching vibration of Si–O–Si bonds. The absorption bands at 1,027 and 512 cm^{-1} are caused by the stretching vibration of Si–O bonds. The absorption peak

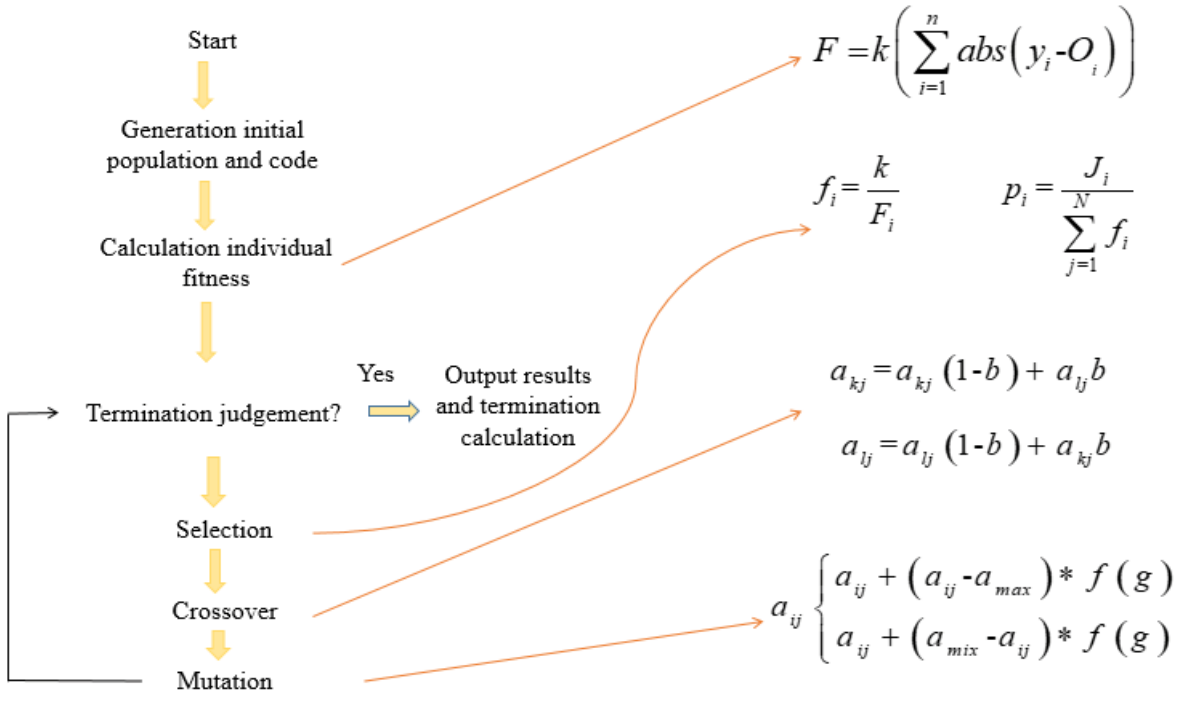

Fig. 2. GA-BP network operation diagram.

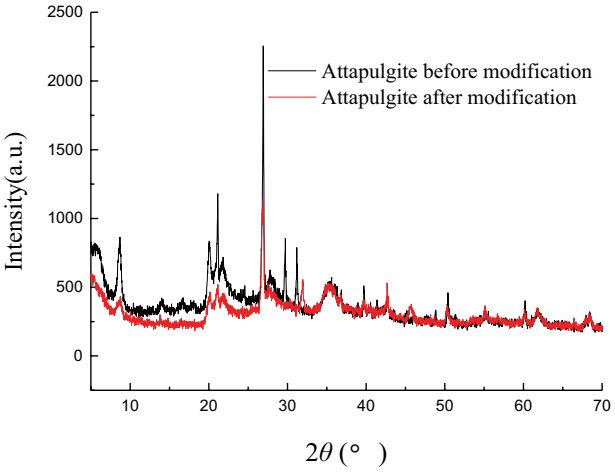

Fig. 3. XRD spectra of attapulgite before and after modification.

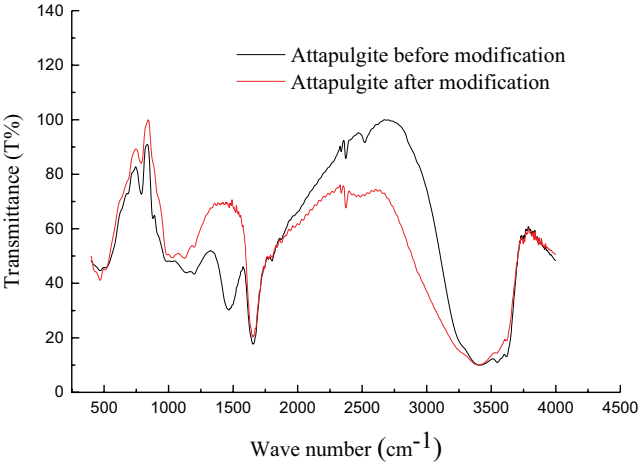

Fig. 4. FI-IR spectra of attapulgite before and after modification.

near 800 cm^{-1} is attributed to the stretching vibration of Si–O–Al bonds.

The microstructure of attapulgite exhibits three layers (Fig. 5). First, the basic structural unit of attapulgite, that is, rod-shaped single crystals, is shown. Then, rod clusters are formed by close and parallel aggregation of rod crystals. Finally, various aggregates are formed by aggregation of rod crystals and rod clusters. After the attapulgite was modified with Keggin ions, the stacking degree of rod crystals decreased, and the material exhibited a loose fibrous crystal structure with a fiber length of 300–700 nm and a diameter of approximately 30–70 nm.

Fig. 6a illustrates that the original soil contains Mg, Al, Si, C, O, and Fe. After adsorption of Cu(II), the Keggin ion-modified attapulgite exhibits a peak of Cu_{2p} in Fig. 6b, and the other elements do not change. Furthermore, according to the high-resolution XPS spectrum of Cu_{2p}, there are three characteristic peaks of Cu_{2p} (933.10, 943.20, and 953.10 eV) after Cu adsorption by the Keggin ion-modified attapulgite (Fig. 6c) [33]. Cu(II) was successfully adsorbed on the modified material. Fig. 6c shows that the C_{1s} spectrum is divided into three peaks corresponding to C=C (284.8 eV),

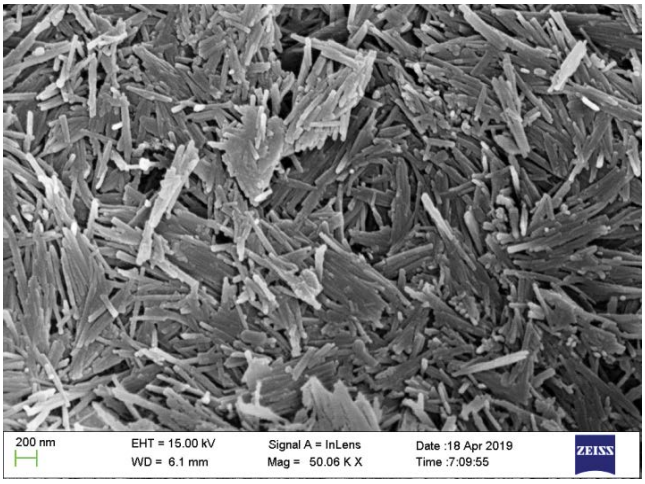

Fig. 5. SEM spectra of attapulgite after modification.

C–OH (286.7 eV), and C=O (288.4 eV) of carboxyl or epoxy groups [34].

3.2. Original attapulgite and attapulgite modified with Keggin ions for Cu(II) removal

To compare the Cu(II) removal efficiency of the two materials, the original attapulgite and attapulgite modified with Keggin ions were employed for Cu(II) removal from aqueous solutions. First, 0.5 g of the original attapulgite was added to a 150 mL triangular bottle containing a Cu(II) concentration of 50 mL. The Cu(II) removal efficiencies of the two materials under fixed conditions (temperature of 25°C, initial Cu(II) concentration of 100 mg/L, initial pH of 7, and contact time of 1–60 min) are exhibited in Fig. 7. The Cu(II) adsorption capability from aqueous solutions using attapulgite modified with Keggin ions was significantly enhanced in comparison with that of the original attapulgite. Because Keggin ions are mainly composed of OH^-/Al^{3+}, the number of OH^- and COO^- groups on the surface of attapulgite will increase after the attapulgite is modified with Keggin ions [35]. Furthermore, complexation reactions can occur between OH^- functional groups and metal ions on the surface of attapulgite. Additionally, heavy metal ions in solution will replace cations in the mineral layer of attapulgite, and ion exchange will occur [36]. Finally, negative COO^- on the surface of attapulgite undergoes electrostatic interactions with positive Cu(II), which was one of the reasons for the successful adsorption of Cu(II).

3.3. BBD for optimizing the process parameters of Cu(II) removal

According to BBD and response surface modeling, a quadratic polynomial model was obtained as follows:

$$F = 76.18 + 1.57A + 0.17B - 2.24C - 2.30D + 1.04AB + 0.99AC - 2.52AD + 2.48BC - 4.44BD - 1.27CD + 1.43A^2 - 4.56B^2 - 0.011C^2 + 3.64D^2 \quad (12)$$

where positive and negative values represent promotion and inhibition of the removal efficiency of Cu(II), respectively.

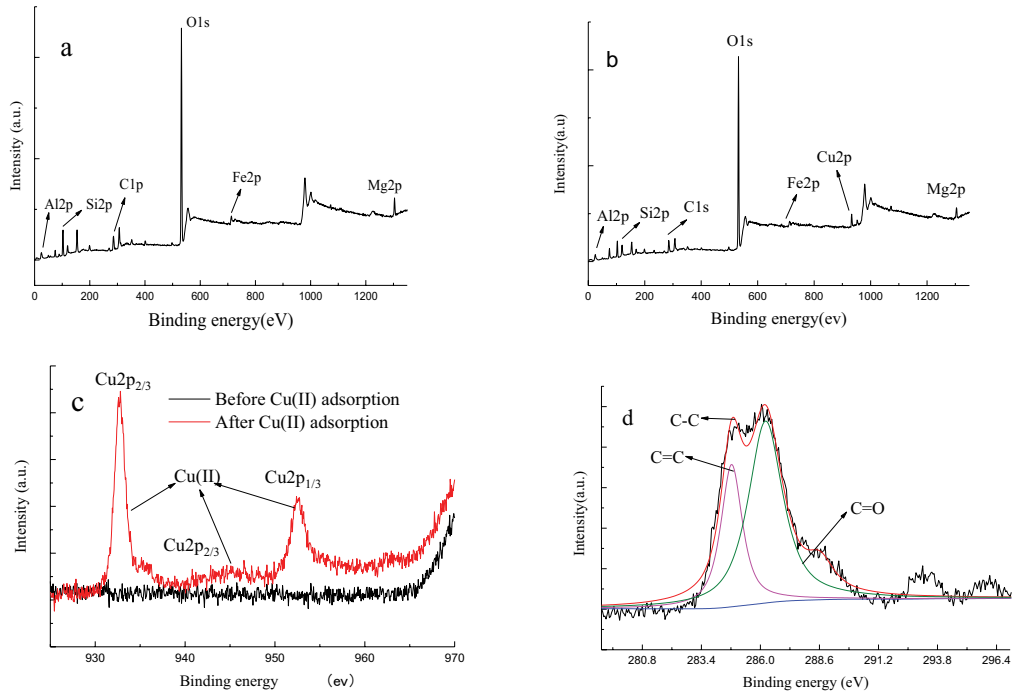

Fig. 6. XPS spectra of Cu(II) adsorbed by modified soils before (a) and after (b), after high resolution adsorption (c), and after high resolution adsorption (d).

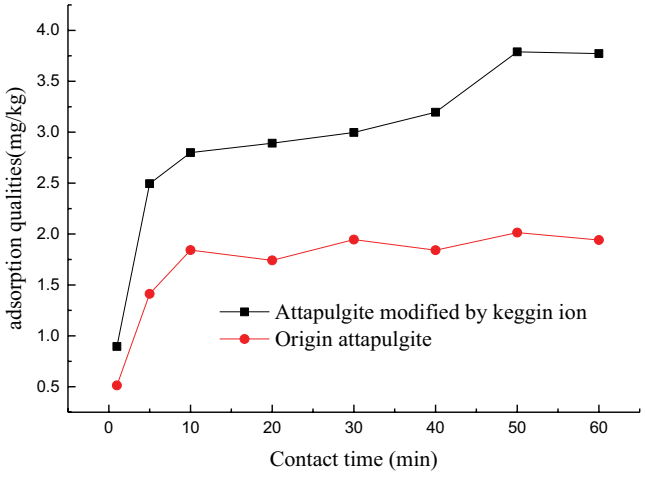

Fig. 7. Origin attapulgite and modified attapulgite by ion for Cu(II) removal (attapulgite dosage = 0.5 g, temperature = 25°C, initial Cu(II) concentration = 100 mg/L, and initial pH = 7).

The order of influence of the four factors on Cu(II) removal was initial pH > initial Cu(II) concentration > reaction time > temperature because the *F* values of *A*, *B*, *C*, and *D* were +1.57, +0.17, –2.24, and 2.30, respectively. The constant (76.18) in the model was not affected by the four factors. The removal efficiency of Cu(II) increased with increases in the linear terms *A* and *B*, quadratic terms *A* and *D*, and interaction terms *AB*, *AC*, and *BC*, while the other terms had the opposite effect.

The developed RSM model is shown in Tables 2 and 3. The significance between the model response values and the regression equation was evaluated by the *p*-value. The low *p*-value ($p \leq 0.0001$) and low lack of fit (0.5395) indicated that the model was significant. A good correlation between the experimental and predicted values was revealed by the high R^2 value (0.9380), which also indicated that the response value of the model has a distinctive relationship with the regression equation. The signal-to-noise ratio can reflect the calculation accuracy of a model, which is generally evaluated by the precision [37]. When the precision is greater than or equal to 4, the model in this study can meet the requirements of the signal-to-noise ratio [38]. The signal-to-noise ratio of the model in Table 3 is greater than Table 4 (15.146), indicating that the calculation results are in good agreement with the test results. In addition, the low coefficient of variation showed that the calculated results of the model coincided with the experimental results. After RSM optimization, the maximum Cu(II) removal efficiency was 87.78% at temperature = 29.49°C, reaction time = 69.92 min, initial pH = 6.00, and initial Cu(II) concentration = 200.00 mg/L. Under these conditions, the actual removal efficiency was 86.28%. Fig. 8 shows the relationship between the internal experimental residuals and normal probability, and Fig. 9 shows the degree of conformity between actual and predicted values. Fig. 10 shows the 3D response surface of the interaction term, which can directly reflect the effects of the interaction term on the removal of Cu(II) from aqueous solutions by Keggin ion-modified attapulgite.

3.4. BP-ANN for optimizing the process parameters of Cu(II) removal

BP is one of the most effective learning methods of multilayer neural networks. The main feature of BP is the

Table 2
Experimental design matrix and results

Code	Contact time (min)	Temperature (°C)	Initial Cu(II) concentration(mg/L)	Initial pH value	Cu(II) removal efficiency (%)	Predicted values (%)	Absolute error (%)
1	70	25	100	7	77.89	76.96	0.93
2	70	25	200	7	75.55	74.46	1.09
3	70	30	150	7	71.30	72.35	1.05
4	60	30	200	7	70.03	71.42	1.39
5	60	25	200	6	81.54	80.54	1.00
6	60	20	100	7	75.62	75.55	0.07
7	60	25	100	6	83.44	82.47	0.97
8	70	25	150	8	75.39	74.53	0.86
9	60	25	100	8	79.84	80.42	0.58
10	50	25	150	8	76.88	76.42	0.46
11	60	25	150	7	73.96	75.56	1.60
12	60	20	150	8	75.40	76.62	1.22
13	60	25	150	7	74.78	75.56	0.78
14	60	30	100	7	69.75	70.94	1.19
15	60	20	150	6	72.20	72.33	0.13
16	60	25	150	7	74.71	75.56	0.85
17	60	25	150	7	76.24	75.56	0.68
18	50	25	150	6	73.80	75.98	2.18
19	60	30	150	8	69.13	68.08	1.05
20	60	20	200	7	66.00	66.13	0.13
21	50	25	200	7	69.33	69.34	0.01
22	60	30	150	6	83.69	81.55	2.14
23	50	30	150	7	67.59	67.13	0.46
24	70	20	150	7	69.90	69.94	0.04
25	50	20	150	7	70.34	68.87	1.47
26	50	25	100	7	75.63	75.80	0.17
27	70	25	150	6	82.38	84.16	1.78
28	60	25	200	8	72.86	73.41	0.55
29	60	25	150	7	78.10	75.56	2.54

forward transmission of the signal and the backward transmission of the error [39]. The final output of the network is made to be as close as possible to the expected output by continuously adjusting the weight value of the network, thereby achieving the purpose of training. The process of the BP-ANN is mainly divided into two stages. The first stage is the forward propagation of the signal from the input layer to the hidden layer and finally to the output layer. The second stage is the back propagation of error from the output layer to the hidden layer and finally to the input layer, successively adjusting the weight and bias from the hidden layer to the output layer and from the input layer to the hidden layer [40]. The neural networks in this study included the three layers, that is, an input layer, hidden layer, and output layer [41] (Fig. 11). The number of neurons in the input layer was the same as the dimension of the input data, and the number of neurons in the output layer was set to 1. The number of neurons in the hidden layer should be set according to the needs of the analysis, and 8 neurons were set in this study. After BP optimization, the maximum removal efficiency was 83.69% at temperature = 30°C, contact time = 60 min, initial pH = 6.83, and initial Cu(II) concentration = 150 mg/L. Under these conditions, the actual removal efficiency was 82.51%.

3.5. GA-BP network for optimizing the process parameters of Cu(II) removal

The simulation performance of the neural network model increased with the number of neurons in the hidden layer. More neurons, however, will lead to overfitting, thus reducing the stability and generalization ability of the neural network model [42]. According to the relationship between the MSE value and the number of neurons, the optimal network structure was determined by using different numbers of neurons in the hidden layer (1–10). Six neurons in the hidden layer were selected in this study (Fig. 12). In our proposed model, several parameters were set, including epoch (2,000), learning rate (0.1), goal ($1e^{-5}$) and momentum factor (0.9) [43]. Fig. 13 shows that the training converged after 1,746 epochs to yield the lowest MSE (0.0014527) for the developed GA-BP model.

Table 3
ANOVA for response surface quadratic model

Source	Sum of squares	Degree of freedom	Mean square	*F*-value	*P*-value	
Model	580.01	14	41.43	15.12	<0.0001	Significant
A	29.58	1	29.58	10.8	0.0054	
B	60.12	1	60.12	21.95	0.0004	
C	0.34	1	0.34	0.13	0.7286	
D	63.25	1	63.25	23.09	0.0003	
AB	4.31	1	4.31	1.57	0.2305	
AC	3.92	1	3.92	1.43	0.2514	
AD	25.35	1	25.35	9.25	0.0088	
BC	24.5	1	24.5	8.94	0.0097	
BD	78.85	1	78.85	28.79	<0.0001	
CD	6.45	1	6.45	2.36	0.1472	
A^2	13.2	1	13.2	4.82	0.0455	
B^2	134.6	1	134.6	49.13	<0.0001	
C^2	7.85×10^{-4}	1	7.85×10^{-4}	2.87×10^{-4}	0.9867	
D^2	86.17	1	86.17	31.46	<0.0001	
Residual	38.35	14	2.74			
Lack of fit	27.55	10	2.75	1.02	0.5395	Not significant
Net error	10.8	4	2.7			
Total dispersion	618.36	28				

R^2 = 0.9380, R^2(adj.) = 0.8760, R^2(pre.) = 0.7161, adequate precision = 15.146 and C.V% = 2.22

Table 4
Kinetics fitting parameters of Cu(II) adsorption onto modified attapulgite

Experimental value	Pseudo-first-order kinetics			Pseudo-second-order kinetics			Intraparticle diffusion model		
q_∞	k_1	q_e	R^2	k_2	q_e	R^2	k_3	C	R^2
3.7724	0.0338	3.2665	0.8710	0.0255	3.6193	0.9806	3.4442	12.407	0.8215

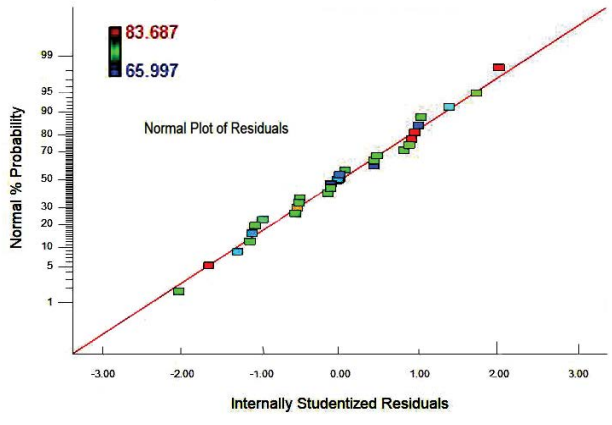

Fig. 8. Internal study of the relationship between residual and normal probability.

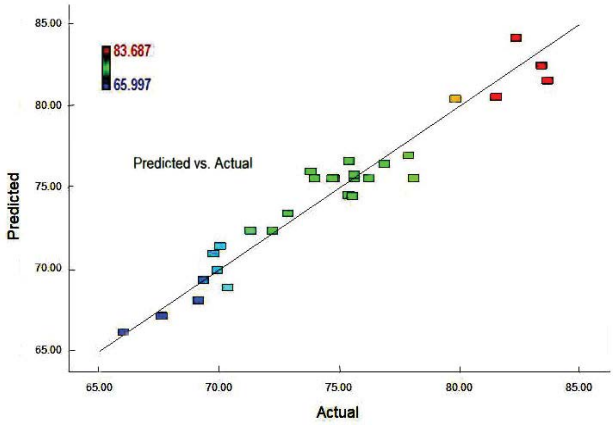

Fig. 9. Relationship between actual and predicted values.

In addition, the R^2 value of the fit between experimental and predicted values was 0.99387, which implied that the established model can meet the prediction requirements. The parameters of GA were set as follows: population size = 20, cross probability = 0.8, mutation probability = 0.01, genetic probability = 0.9, and maxgen = 500 [43].

Based on the model developed by GA-BP, the Cu(II) removal efficiency in aqueous solutions by Keggin ion-

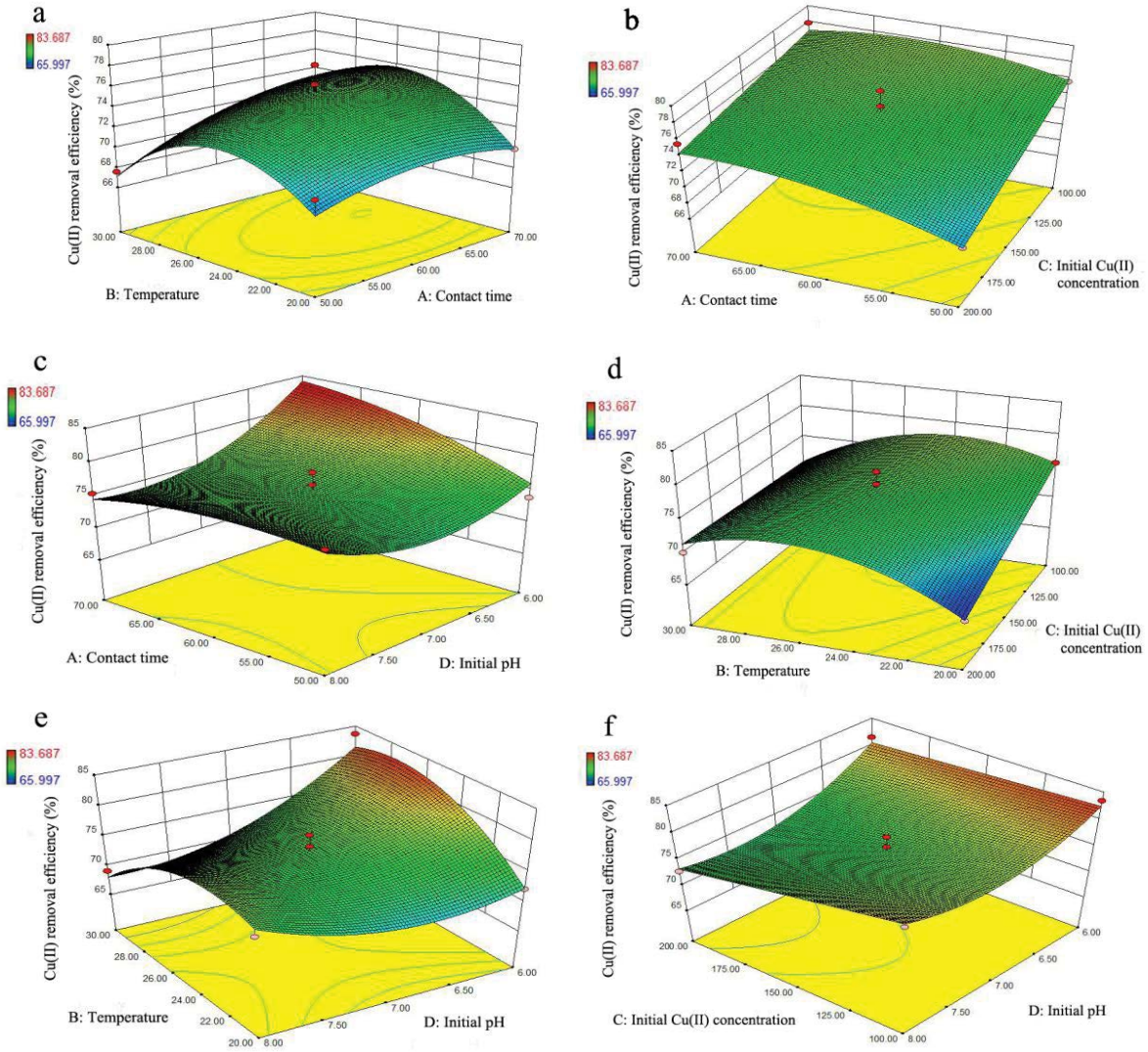

Fig. 10. (a–f) Relationship between removal rate and experimental parameters.

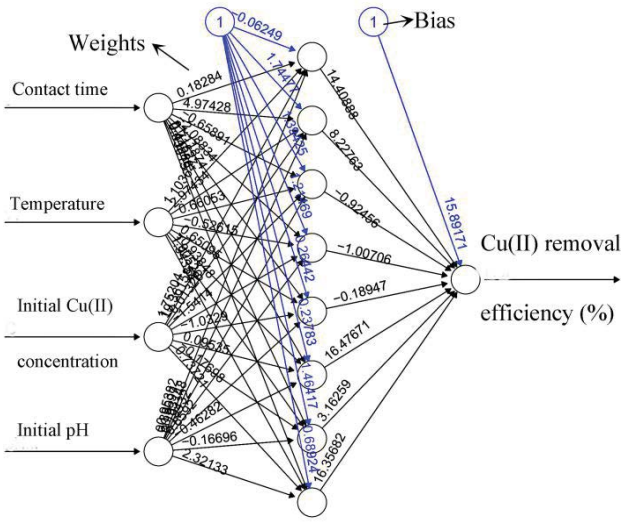

Fig. 11. BP structure diagram under R language running.

modified attapulgite was predicted to be the highest at approximately 250 iterations (Fig. 12). The maximum removal efficiency of Cu(II) was 91.35% at a temperature of 29.73°C, contact time of 69.60 min, initial pH of 6.46, and initial Cu(II) concentration of 100.00 mg/L. Under these conditions, the actual removal efficiency was 90.06% (Fig. 14).

3.6. Factor importance analysis

Random forest is an integrated learning algorithm based on a decision tree [44]. The RF algorithm in machine learning can output the importance of each feature after the model is trained. The importance of the attribute can be judged by the obtained feature importance (Fig. 15). The order of importance of influencing factors was initial pH value > temperature > initial Cu(II) concentration > contact time.

ABT, based on stacked probability boosting mode, was used for the evaluation of the factor importance using the gbmplus function package in *R* [45]. The relative influence

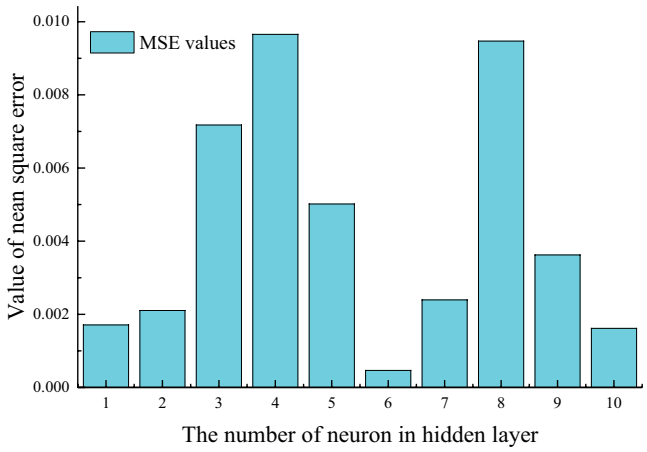

Fig. 12. Relationship between neurons and MSE values.

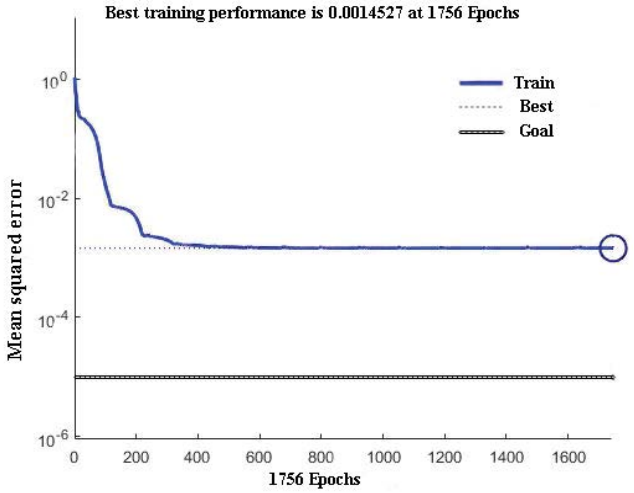

Fig. 13. Correlation between the number of iterations and MSE.

between independent variables and dependent variables can be eliminated through the relative importance diagram. Fig. 16 shows that the contribution to removal efficiency of each influencing factor was as follows: initial pH value (33.15%) > temperature (32.54%) > initial Cu(II) concentration (18.93%) > reaction time (15.37%).

3.7. Kinetics study

Pseudo-first-order kinetics, pseudo-second-order kinetics, and the intraparticle diffusion model were used to study the rate-controlling steps and adsorption mechanism [46].

Pseudo-first-order kinetics:

$$\ln\left(q_e - q_t\right) = \ln q_e - k_1 t \tag{13}$$

Pseudo-second-order kinetics:

$$\frac{t}{q_t} = \frac{1}{k_2 q_e^2} + \frac{t}{q_e} \tag{14}$$

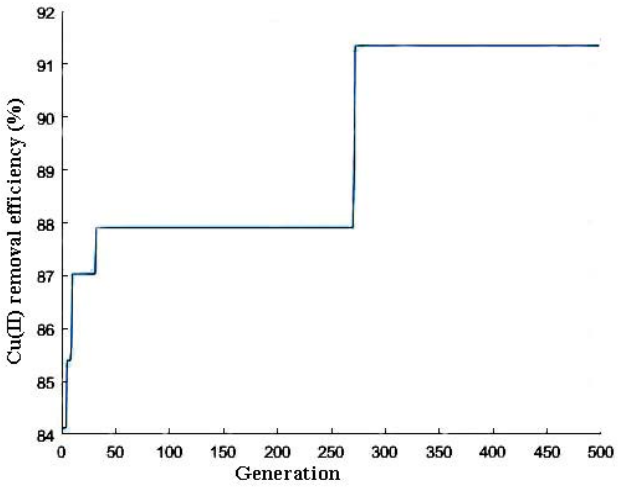

Fig. 14. Fitting the predicted value under 500 iterations.

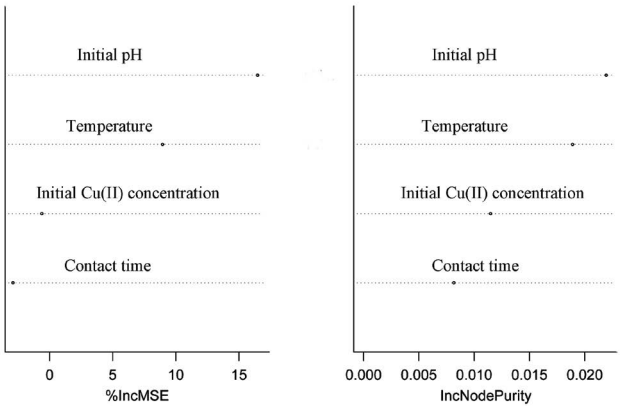

Fig. 15. Importance of random forest assessment characteristics.

Intraparticle diffusion model:

$$q_t = k_{id} t^{1/2} + C \tag{15}$$

where q_e is the equilibrium adsorption capacity, mg/g; q_t is the adsorption capacity at t, mg/g; k_1 is the adsorption rate constant of the pseudo-first-order kinetic equation, h^{-1}; k_2 is the adsorption rate constant of the pseudo-second-order kinetic equation, g/(mg h); k_{id} (mg/g/min$^{1/2}$) is the intraparticle diffusion rate constant; and C is a constant. All heavy metals exhibit a larger slope at a lower equilibrium concentration (Fig. 17). The adsorption quantities of heavy metals increased with contact time. The removal quantity of Cu(II) were the largest, followed by those of As(III), Pb(II), and Hg(II), which were dramatically adsorbed and then slowly adsorbed. The reason may be that the adsorption sites on the surface of the modified attapulgite gradually became saturated with increasing contact time [47]. However, the capacity of each heavy metal to combine with the modified attapulgite was different since these heavy metals have different properties. Hence, the maximum adsorption capacity of each heavy metal differed substantially, among which Cu(II) exhibited the most obvious

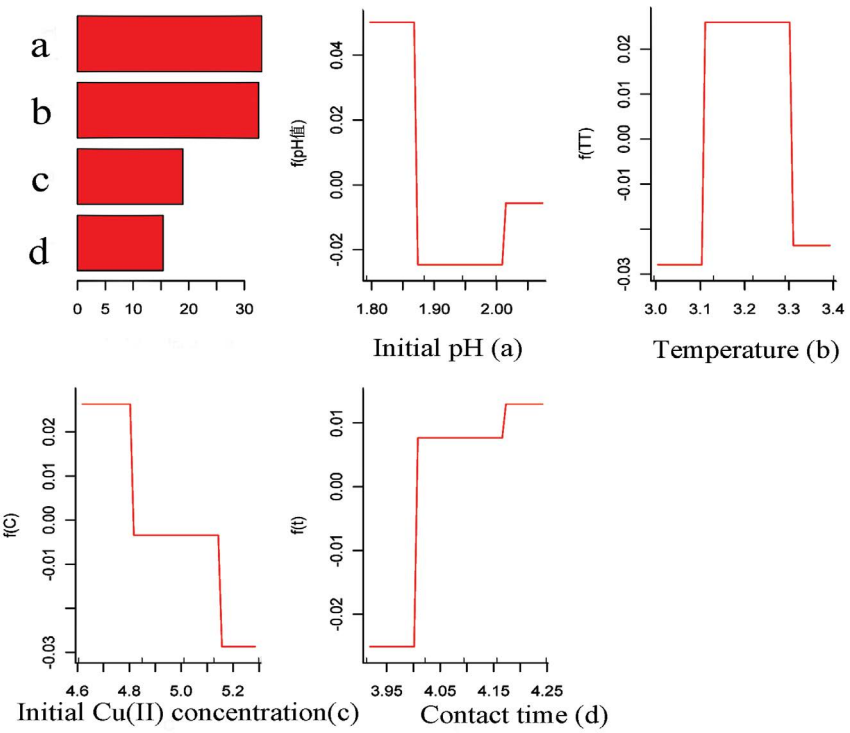

Fig. 16. Importance of APT assessment characteristics. (a) Initial pH, (b) temperature, (c) initial Cu(II) concentration, and (d) contact time.

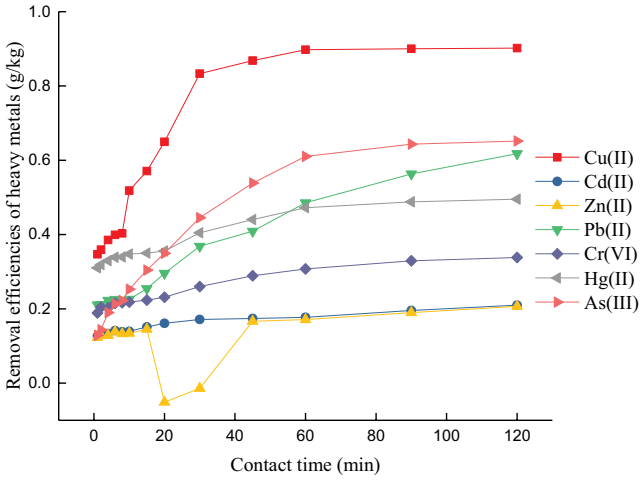

Fig. 17. Adsorption quantity of Cu(II) by modified attapulgite at different time (attapulgite dosage = 0.5 g, temperature = 25°C, initial heavy metals concentration = 50 mg/L, and initial pH = 7).

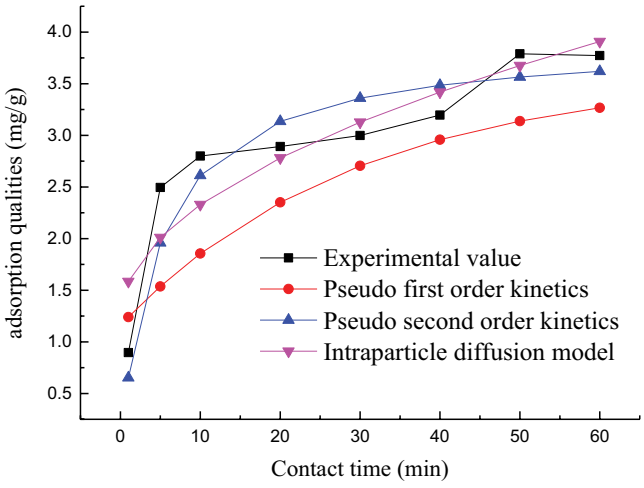

Fig. 18. Adsorption quantity of Cu(II) by modified attapulgite at different time (attapulgite dosage = 0.5 g, temperature = 25°C, initial Cu(II) concentration = 100 mg/L, and initial pH = 7).

effect with increasing contact time. In this study, Cu(II) was selected for specific discussion due to the sensitivity of Cu(II) adsorption by the modified attapulgite.

Pseudo-second-order kinetics can well describe the adsorption behavior of Cu(II) on the modified soil surface because of the high R^2 value (0.9806) and low absolute error between the fitted value (3.6193 mg/g) and the experimental value (3.7724 mg/g). According to the adsorbed amounts of Cu(II) by the modified soil at different contact times (Fig. 18), the adsorbed amount of Cu(II) by the modified soil increased rapidly in a short time, and then there was a relatively gentle change trend, reaching equilibrium at approximately 60 min. The adsorption capacity of the modified soil for Cu(II) reached approximately one-third of the equilibrium adsorption capacity within 10 min, and the Cu(II) adsorbed amount slowly increased after 50 min. This phenomenon may be due to the higher concentration of Cu(II) in the initial stage and the stronger concentration driving force, which increased the contact probability between Cu(II) and the surface of the modified soil [48].

Additionally, there were many adsorption sites on the surface of the modified soil at the beginning of the adsorption experiment with a strong adsorption capacity for Cu(II). Equilibrium was gradually approached as the reaction progressed. The lower the number of adsorption sites was, the lower the adsorption capacity was [49]. In addition, dynamic equilibrium between desorption and adsorption was reached, and the reaction may be dominated by chemical adsorption [50]. It was found that the slope of the first part of the fitting curve was larger than that of the second part. The slope of the former part indicated the transfer of Cu(II) from the Cu(II)-containing solutions to the surface of the modified soil, and the latter part corresponded to internal diffusion. This result showed that internal diffusion was not a process limiting the adsorption rate.

3.8. Adsorption isotherm study

The Langmuir, Freundlich, and Temkin adsorption isotherm models were employed to investigate the nature of Cu(II) removal by adsorption [51].

Langmuir adsorption isotherm model:

$$\frac{C_e}{q_e} = \frac{1}{K_L q_{\max}} + \frac{C_e}{q_{\max}} \tag{16}$$

Freundlich adsorption isotherm model:

$$\ln q_e = \ln K_F + \frac{1}{n}\ln C_e \tag{17}$$

Temkin adsorption isotherm model:

$$q_e = B\ln\left(AC_e\right)$$
$$B = RT/b \tag{18}$$

where C_e is the adsorption equilibrium concentration, mg/L; q_e is the adsorption amount at equilibrium concentration, mg/g; $q_{\max}$ is the maximum adsorption amount at saturation(mg/g); K_L (L/mg) is the binding constant of the Langmuir adsorption model, L/mg; K_F (mg/g) is the Freundlich constant; $1/n$ is the Freundlich adsorption intensity parameter; A (L/g) is the binding constant corresponding to the maximum binding energy; and B (J/mol), R, T, and b are the Temkin constant, gas constant, absolute temperature, and adsorption heat, respectively.

Adsorption isotherms are an important method in the design of adsorption processes and are used to describe the equilibrium relationship between the adsorbent and adsorbate and the affinity and adsorption capacity of the adsorbent [52]. The Langmuir model assumes that the adsorbent surface is homogeneous and there are no interactions between particles, so monolayer adsorption occurs [53]. The Freundlich model assumes that the enthalpy of adsorption is distributed unevenly on the adsorbent surface and increases with surface coverage [54]. The Temkin model is a real adsorption model that assumes that the adsorption heat on the surface of the adsorbent decreases linearly with increasing coverage [55]. However, the Temkin model is not suitable for cases with a high vapor pressure or coverage of adsorbate. The Langmuir, Freundlich, and Temkin models were used to fit the experimental data from the adsorption process. According to Table 5 and Fig. 19, the Langmuir isotherm model was the most suitable to describe the adsorption process of Cu(II) onto the surface of the modified soil. The process of surface adsorption involved a single molecular layer, and the maximum adsorption capacity was 6.5675 mg/g. The term $1/n$ can be used to describe the degree of deviation of adsorption from linearity. Values of $1/n > 2$ and $0.1 < 1/n < 2$ indicate that adsorption is difficult and easy, respectively. The modified soil easily adsorbed Cu(II) in this study because $1/n$ was 0.6672. In addition, the low K_F value (1.1477) indicated that the adsorption capacity of the modified soil for Cu(II) was weak [54]. A value of RT/b = 203.22 was obtained from Temkin model, which indicated that the adsorption process included both physical and chemical adsorption [55] (Table 5).

3.9. Thermodynamic analysis

The change in Gibbs free energy related to a chemical reaction can be used to evaluate the spontaneity of the reaction process [56]. The Gibbs equation was used to calculate the thermodynamic functions in this study.

$$\ln K_T = \frac{\Delta S^\circ}{R} - \frac{\Delta H^\circ}{RT} \tag{19}$$

$$\Delta G^\circ = -RT\ln K_T \tag{20}$$

$$K_T = \frac{C_0}{C_e} \tag{21}$$

where ΔG° is the standard adsorption free energy change. ΔH° is the standard adsorption enthalpy change. ΔS° is the standard adsorption entropy change. R is the gas constant, 8.314 J/(mol K). T is the absolute temperature, and K_T is the adsorption coefficient. The values of ΔH° and ΔS° were 10.715 kJ/mol and 48.5739 J/(mol K), respectively (Table 6). The adsorption process was spontaneous due to $\Delta G^\circ < 0$ in this study. The value of ΔG° decreases with increasing

Table 5
Adsorption isotherm fitting parameters of Cu(II) adsorption onto modified attapulgite

Langmuir model			Freundlich model			Temkin model		
$q_{\max}$	K_L	R^2	K_F	$1/n$	R^2	a	b	R^2
6.5675	0.0203	0.9481	1.1477	0.6672	0.9806	12.198	1.1961	0.8536

Table 6
Thermodynamic state function values of adsorption of Cu(II) by modified attapulgite

$\Delta H°$ (kJ/mol)	$\Delta S°$ (J/(mol K))	$\Delta G°$ (kJ/mol)					
		293.15 K	298.15 K	303.15 K	308.15 K	313.15 K	318.15 K
10.715	48.5739	–3.7896	–4.0728	–4.2814	–4.6891	–4.7748	–5.016

absolute temperature since an increase in temperature can promote the dehydration of hydrated metal ions, making it easier for Cu(II) to interact with the active sites on the surface of the modified soil [57]. The adsorption process of Cu(II) onto the surface of the modified soils was endothermic due to $\Delta H° > 0$, and an increase in temperature was conducive to the reaction. In addition, solute adsorption and solvent desorption will occur in a solid/liquid adsorption system [58]. The former will reduce the degrees of freedom, that is, the process of entropy reduction, and the latter is the process of entropy increase. The entropy of an adsorption process is the sum of solute adsorption and solvent desorption [59]. Therefore, the entropy value of a process may be negative or positive. The entropy change for Cu(II) adsorption onto the surface of the modified soil was greater than 0, which indicated that the entropy increase caused by solvent desorption was greater than that caused by Cu(II) adsorption, thus increasing the degree of disorder of the adsorption system [60].

The adsorption qualities of Cu(II) from simulated wastewater removal by the modified attapulgite was improved with the increase of temperature. The number of adsorption sites on the surface of adsorption materials will increase with the increase of temperature, thus increasing the contact between heavy metal ions and adsorption sites on the surface of adsorption materials (Fig. 20) [61]. Therefore, the increase of temperature can increase the adsorption capacity of attapulgite to Cu(II) in solution.

3.10. Influence of pH value on Cu(II) removal efficiency

The free energy and active groups on the surface of an adsorbent are significantly affected by different acidities (Fig. 21). The surface energy and form of a solute in solution will also change, which determines the different adsorption capacities of adsorbents for solutes at different pH values [62]. Although the efficiency of Cu(II) removal by the modified attapulgite continuously increased from pH values of 2–12, the value was relatively low at pH < 6. The reason may be that Cu(II) and H^+ competed for the adsorption sites of the surface of the modified attapulgite at higher acidity in solution. The efficiency of Cu(II) removal by the attapulgite modified with Keggin ions was relatively high at pH > 8, which may be caused by the main form of Cu(II) being hydroxyl-coordination ions ($Cu(OH)^+$) in alkaline solutions. Hydrolyzed metal ions of multivalent metal ions are more easily adsorbed than non-hydrolysed metal ions by the solid particles in solution.

3.11. Regeneration of the attapulgite modified with keggin ions

The regeneration of an adsorbent is an important factor in assessing its possibility for practical applications. Cu(II)

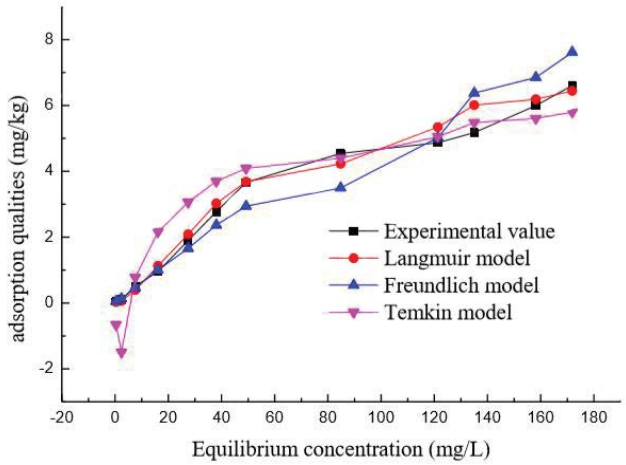

Fig. 19. Adsorption quantity of Cu(II) by the modified attapulgite at equilibrium concentration (attapulgite dosage = 0.5 g, temperature = 25°C, contact time = 60 min, and initial pH = 7).

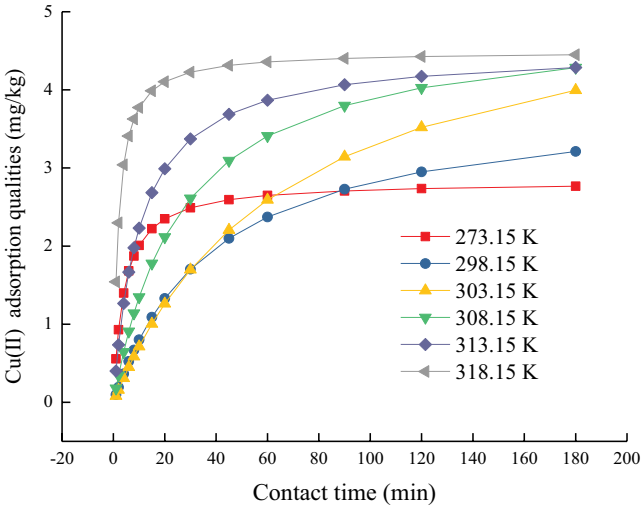

Fig. 20. Temperature influencing on the Cu(II) adsorption qualities (attapulgite = 0.5 g, contact time = 60 min, initial Cu (II) concentration = 100 mg/L, and initial pH value = 7).

adsorption was repeated for three cycles using an eluent of 0.1 mol/L HCl. As shown in Fig. 23, the removal efficiencies of the first regeneration cycle, second regeneration cycle, third regeneration cycle, and fourth regeneration cycle were 92.36%, 89.24%, 85.98%, and 79.25%, respectively. This result reveals that a gradual decline in the adsorption capacity of the attapulgite modified with Keggin ions for Cu(II) for four consecutive adsorption cycles, and a dramatic decline

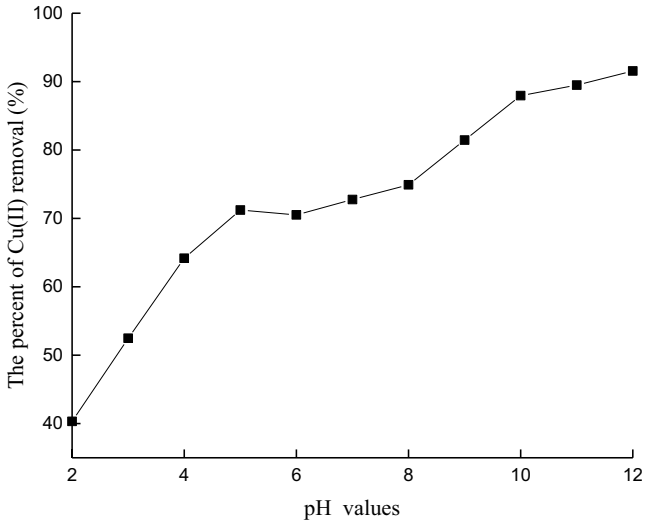

Fig. 21. pH value influencing on the Cu(II) removal efficiency (attapulgite = 0.5 g, temperature = 25°C, contact time = 60 min, and initial Cu(II) concentration = 100 mg/L).

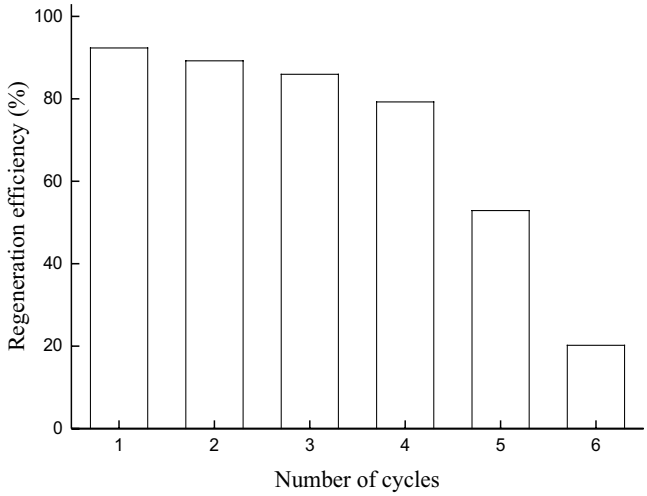

Fig. 22. Evolution of regeneration efficiency after each regeneration cycle (attapulgite = 0.5 g, temperature = 25°C, contact time = 60 min, initial Cu(II) concentration = 100 mg/L, and initial pH = 7).

was observed after four regeneration cycles, indicating that attapulgite modified with Keggin ions is an effective and reusable adsorbent. Although the lower maximum adsorption capacity of Cu(II) in comparison with the other literatures, the modified attapulgite is still of huge potential application in environmental remediation because of the cheap and easy raw material (Table 7).

4. Conclusion

The present study used Keggin ions to modify attapulgite to improve the removal efficiency of Cu(II) at high concentrations in aqueous solutions. XRD analysis showed that the structure of attapulgite did not change prominently after Keggin ion modification. XPS revealed that Cu(II) was successfully adsorbed on the modified attapulgite. According to the experimental results, the Cu(II) adsorption capability from aqueous solutions using attapulgite modified with Keggin ions was dramatically enhanced in comparison with that of the original attapulgite. In summary, GA-BP was the most suitable approach for modeling Cu(II) removal from aqueous solutions because its absolute error between experimental and predicted values was the smallest. According to GA-BP optimization, the maximum removal efficiency of Cu(II) was 91.35% at a temperature of 29.73°C, contact time of 69.60 min, initial pH of 6.46, and initial Cu(II) concentration of 100.00 mg/L. The three analysis methods (analysis of variance, ABT, and random forest) revealed that initial pH was the most influential variable in Cu(II) removal from aqueous solutions. The fitting results showed that the Langmuir isotherm and pseudo-second-order kinetic model could describe the adsorption process, which was a spontaneous and entropy-driven process. The mechanism study on the removal of Sb(III) demonstrated that the adsorption process was accompanied by a redox reaction. The regeneration experiments showed that the attapulgite modified with Keggin ions for Cu(II) removal from simulated wastewater are an effective and reusable adsorbent within four regeneration cycles.

Table 7
Comparison of the adsorption capacity for Cu(II) on the modified attapulgite by Keggin ions with those of other adsorbents

Materials	Cycles	Maximum adsorption capacity	References
Poly(amidoamine) dendrimer-functionalized nanocrystalline cellulose composites	5	92.07 mg/g	[63]
NaP zeolite	3	69.93 mg/g	[64]
Porous hydroxyapatite	ND	69.90 mg/g	[65]
Iranian natural zeolite	ND	4.70 mg/g	[66]
Bentonite (coated with magnetite Fe_3O_4)	3	46.95 mg/g	[67]
Coconut tree sawdust	ND	3.89 mg/g	[68]
Sugarcane bagasse	ND	3.65 mg/g	[68]
Activated carbon prepared from Hazelnut husk	4	6.65 mg/g	[69]
The modified attapulgite by Keggin ions	4	3.77 mg/g	This study

"ND" represents no data.

To further explore the mechanism of the adsorption process, X-ray absorption near edge structure (XANES) analysis based on synchrotron radiation could be used to identify the local atomic environment (i.e., valence and coordination) of Cu(II) before and after the adsorption of Cu(II) onto the modified attapulgite. Synchrotron radiation is produced when high-energy particles, including electrons, are accelerated and forced to travel in a curved path by a magnetic field. Small-angle XRD analysis could also be used to obtain information concerning the state (e.g., ordered mesopores) of the samples on a nanometre scale. Finally, the reuse potential of these nanocomposites should be investigated to reduce costs, and a scaled-up system (e.g., permeable reactive barrier) needs to be developed for Cu(III) removal with the aid of more advanced optimizing techniques.

Author Contributions

WX, CC, and CS designed and wrote the research; WX wrote the paper; TC, LQ, and ZZ performed the experiments and data analysis.

Acknowledgments

This research was financially supported by Environmental Engineering Subject with Open-End Fund in Key Laboratory in Jiangsu Province for Scientific Research (KF2015013), Surface Project of Scientific Research of Institutions of Higher Learning in Jiangsu Province (17KJB610002), Environmental Engineering Subject with Open-End Fund in Key Laboratory in Jiangsu Province for Scientific Research (KF2015005), the 100 High Level Innovating Project (Grant No. QKHRC-2016-5666), and the Science and Technology Plan Project of Guizhou Province (GZKJ [2019]2840).

References

[1] M. Ogórek, Ł. Gąsior, O. Pierzchała, R. Daszkiewicz, M. Lenartowicz, Role of copper in the process of spermatogenesis, Postepy Hig. Med. Dosw., 71 (2017) 663–670.
[2] A.K. Szczepanska, K. Malinowska, I. Majsterek, An evaluation of the antioxidant and anticancer properties of complex compounds of copper(II), platinum(II), palladium(II) and ruthenium(III) for use in cancer therapy, Mini Rev. Med. Chem., 18 (2018) 1373–1381.
[3] O. Kaplan, G. Kaya, M. Yaman, Sequential and selective extraction of copper in different soil phases and plant parts from former industrialized area, Commun. Soil Sci. Plant Anal., 42 (2011) 2391–2401.
[4] J. Zhang, The compare of different determine methods for cuprum content, Port Health Control, 6 (2001) 22–23 (in Chinese).
[5] M. Malik, A. Mansur, Copper sulphate poisoning and exchange transfusion, Saudi J. Kidney Dis. Transpl., 22 (2011) 1240–1242.
[6] W. Liu, T. Yang, J. Xu, Q. Chen, C. Yao, S. Zuo, Y. Kong, C. Fu, Preparation and adsorption property of attapulgite/carbon nanocomposite, Environ. Prog. Sustainable Energy, 34 (2015) 437–444.
[7] Y. Feng, Y. Wang, Y. Wang, S. Liu, J. Jiang, C. Cao, J. Yao, Simple fabrication of easy handling millimeter-sized porous attapulgite/polymer beads for heavy metal removal, J. Colloid Interface Sci., 502 (2017) 52–58.
[8] T. Falayi, F. Ntuli, Effect of attapulgite calcination on heavy metal adsorption from acid mine drainage, Korean J. Chem. Eng., 32 (2015) 707–716.
[9] Y.W. Zheng, W.W. Tao, G.F. Zhang, C. Lv, Y.P. Zhao, L. Chen, Adsorptive removal of Ni(II) ions from aqueous solution by polyacrylic acid/attapulgite composite hydrogels, Key Eng. Mater., 727 (2017) 859–865.
[10] J.D. Sudha, A. Pich, V.L. Reena, S. Sivakala, H.J.P. Adler, Water-dispersible multifunctional polyaniline-laponite-keggin iron nanocomposites through a template approach, J. Mater. Chem., 21 (2011) 16642–16650.
[11] G.I. Danmaliki, T.A. Saleh, A.A. Shamsuddeen, Response surface methodology optimization of adsorptive desulfurization on nickel/activated carbon, Chem. Eng. J., 313 (2017) 993–1003.
[12] H. Guan, Z. Dai, A. Zhao, J. He, A novel stock forecasting model based on high-order-fuzzy-fluctuation trends and back propagation neural network, PLoS One, 13 (2018) e0192366–e0192372, doi: 10.1371/journal.pone.0192366.
[13] N. Zhang, K. Zhou, L. Dong, Back-propagation neural network and support vector machines for gold mineral prospectivity mapping in the Hatu region, Xinjiang, China, Earth Sci. Inform., 11 (2018) 553–566.
[14] Y. Zhang, X.U. Jinrui, F.U. Xinghu, J. Liu, Y. Tian, Hybrid algorithm combining genetic algorithm with back propagation neural network for extracting the characteristics of multi-peak Brillouin scattering spectrum, Front. Optoelectron., 10 (2017) 62–69.
[15] L. Zhuo, J. Zhang, P. Dong, Y. Zhao, B. Peng, An SA–GA–BP neural network-based color correction algorithm for TCM tongue images, Neurocomputing, 134 (2014) 111–116.
[16] R. Hazime, Q.H. Nguyen, C. Ferronato, T.K.X. Huynh, J.M. Chovelon, Optimization of imazalil removal in the system UV/TiO_2/$K_2S_2O_8$ using a response surface methodology (RSM), Appl. Catal., B, 132–133 (2013) 519–526.
[17] M. Liu, X. Liu, M. Li, M. Fang, W. Chi, Neural-network model for estimating leaf chlorophyll concentration in rice under stress from heavy metals using four spectral indices, Biosyst. Eng., 106 (2010) 223–233.
[18] A.R. Awad, I. Von Poser, M.T. Aboul-Ela, Optimal removal of heavy metals pollutants from groundwater using a real genetic algorithm and finite-difference method, J. Comput. Civil Eng., 27 (2013) 522–533.
[19] Y. Ge, J.Z. He, Y.G. Zhu, J.B. Zhang, Z. Xu, L.M. Zhang, Y.M. Zheng, Differences in soil bacterial diversity: driven by contemporary disturbances or historical contingencies?, ISME J., 2 (2008) 254–264.
[20] J.Z. He, Y. Ge, Z. Xu, C. Chen, Linking soil bacterial diversity to ecosystem multifunctionality using backward-elimination boosted trees analysis, J. Soils Sediments, 9 (2009) 547–550.
[21] M. Shanmugaprakash, J. Kirthika, J. Ragupathy, K. Nilanee, A. Manickam, Statistical based media optimization and production of naringinase using *Aspergillus brasiliensis* 1344, Int. J. Biol. Macromol., 64 (2014) 443–452.
[22] M. Hesham, P. Bruno, S. Sadique, C. Gert, Hardware-efficient on-line learning through pipelined truncated-error backpropagation in binary-state networks, Front. Neurosci., 11 (2017) 496–504.
[23] S. Ding, C. Su, J. Yu, An optimizing BP neural network algorithm based on genetic algorithm, Artif. Intell. Rev., 36 (2011) 153–162.
[24] D. Zhang, J. Xu, C. Li, Model for food safety warning based on inspection data and BP neural network, Trans. Chin. Soc. Agric. Eng., 26 (2010) 221–226 (in Chinese).
[25] L.X. Guo, M.Y. Zhao, A parallel search genetic algorithm based on multiple peak values and multiple rules, Mech. Technol., 129 (2002) 539–544.
[26] U. Maulik, S. Bandyopadhyay, Genetic algorithm-based clustering technique, Pattern Recognit., 33 (2000) 1455–1465.
[27] Y. Fei, H. Mao, L. Hua, A hybrid of back propagation neural network and genetic algorithm for optimization of injection molding process parameters, Mater. Des., 32 (2011) 3457–3464.
[28] Z. Niu, Q. Fan, W. Wang, J. Xu, L. Chen, W. Wu, Effect of pH, ionic strength and humic acid on the sorption of uranium(VI) to attapulgite, Appl. Radiat. Isot., 67 (2009) 1582–1590.
[29] F. Gourbilleau, C. Ternon, D. Maestre, O. Palais, C. Dufour, Silicon-rich SiO_2/SiO_2 multilayers: a promising material for

the third generation of solar cell, J. Appl. Phys., 106 (2009) 13501–13507.
[30] A. Saito, A. Kawakami, H. Shimakage, Z. Wang, As-grown MgB_2 thin films deposited on Al_2O_3 substrates with different crystal planes, Supercond. Sci. Technol., 15 (2002) 1325–1330.
[31] H. Xu, P.J. Heaney, G.H. Beall, Phase transitions induced by solid solution in stuffed derivatives of quartz: a powder synchrotron XRD study of the $LiAlSiO_4$-SiO_2 join, Am. Mineral, 85 (2015) 971–979.
[32] P.P. Kundu, R.C. Larock, Montmorillonite-filled nanocomposites of tung oil/styrene/divinylbenzene polymers prepared by thermal polymerization, J. Appl. Polym. Sci., 119 (2011) 1297–1306.
[33] M.Y. Fan, J.W. Hu, R.S. Cao, K.N. Xiong, X.H. Wei, Modeling and prediction of copper removal from aqueous solutions by nZVI/rGO magnetic nanocomposites using ANN-GA and ANN-PSO, Sci. Rep., 7 (2017) 18040–18047.
[34] R.S. Cao, M.Y. Fan, J.W. Hu, W.Q. Ruan, K.N. Xiong, X.H. Wei, Optimizing low-concentration mercury removal from aqueous solutions by reduced graphene oxide-supported Fe_3O_4 composites with the aid of an artificial neural network and genetic algorithm, Materials, 10 (2017) 1279–1285.
[35] W. Wang, M. Amiri, K. Kozma, Reaction pathway to the inaugural open-shell transition-metal Keggin ion without organic ligation, Eur. J. Inorg. Chem., 2018 (2018) 4638–4642.
[36] M. Igawa, S. Akiyama, R. Okada, C. Sugawara, T. Kurokawa, Separation of heavy metal Ions with a chelating reagent fixed in an anion-exchange membrane, J. Ion Exch., 18 (2007) 506–509.
[37] W.Q. Ruan, J.W. Hu, J.M. Qi, Y. Hou, R.S. Cao, X.H. Wei, Removal of crystal violet by using reduced-graphene-oxide-supported bimetallic Fe/Ni nanoparticles (rGO/Fe/Ni): application of artificial intelligence modeling for the optimization process, Materials, 11 (2018) 865–872.
[38] M.Y. Fan, T.J. Li, J. W. Hu, Synthesis and characterization of reduced graphene oxide-supported nanoscale zero-valent iron (nZVI/rGO) composites used for Pb(II) removal, Materials, 9 (2016) 687–695.
[39] M.Y. Fan, J.W. Hu, R.S. Cao, W.Q. Ruan, X.H. Wei, A review on experimental design for pollutants removal in water treatment with the aid of artificial intelligence, Chemosphere, 200 (2018) 330–343.
[40] E. Yan, J. Song, C. Liu, Comparison of support vector machine, back propagation neural network and extreme learning machine for syndrome element differentiation, Artif. Intell. Rev., 53 (2019) 2453–2481.
[41] H. Mustafidah, S. Suwarsito, Correlation analysis between error rate of output and learning rate in backpropagation network, Adv. Sci. Lett., 24 (2018) 9182–9185.
[42] V. Couvreur, M.M. Kandelous, B.L. Sanden, Downscaling transpiration rate from field to tree scale, Agric. For. Meteorol., 221 (2016) 71–77.
[43] R.S. Cao, M.Y. Fan, J.W. Hu, W.Q. Ruan, X.L. Wu, X.H. Wei, Artificial intelligence based optimization for the Se(IV) removal from aqueous solution by reduced graphene oxide-supported nanoscale zero-valent iron composites, Materials, 11 (2018) 428–439.
[44] H. Norouzi, S. Shahmohammadi-Kalalagh, Locating ground-water artificial recharge sites using random forest: a case study of Shabestar region, Iran, Environ. Geol., 78 (2019) 380–391.
[45] B. He, D. Xiao, Q. Hu, Automatic magnetic resonance image prostate segmentation based on adaptive feature learning probability boosting tree initialization and CNN-ASM refinement, IEEE Access, 6 (2018) 2005–2015.
[46] C. Chen, T. Cheng, Y.S. Shi, Y. Tian, Adsorption of Cu(II) from aqueous solution on fly ash based linde F (K) Zeolite, Iran, J. Chem. Chem. Eng., 33 (2014) 29–35.
[47] C. Chen, T. Cheng, Z.L. Wang, C.H. Han, Removal of Zn^{2+} in aqueous solution by Linde F (K) zeolite prepared from recycled fly ash, J. Indian Chem. Soc., 91 (2014) 1–7.
[48] F.C. Wu, R.L. Tseng, R.S. Juang, Initial behavior of intraparticle diffusion model used in the description of adsorption kinetics, Chem. Eng. J., 153 (2009) 1–8.
[49] G. Postole, A. Auroux, The poisoning level of Pt/C catalysts used in PEM fuel cells by the hydrogen feed gas impurities: the bonding strength, Int. J. Hydrogen Energy, 36 (2011) 6817–6825.
[50] T. Wang, K.S. Lackner, A.B. Wright, Moisture-swing sorption for carbon dioxide capture from ambient air: a thermodynamic analysis, Phys. Chem. Chem. Phys., 15 (213) 504–512.
[51] T. Cheng, C. Chen, R. Tang, C.H. Han, Y. Tian, Competitive adsorption of Cu, Ni, Pb, and Cd from aqueous solution onto fly ash-based Linde F(K) zeolite, Iran, J. Chem. Chem. Eng., 37 (2018) 61–71.
[52] C. Chen, T. Cheng, X. Zhang, R.X. Wu, Q.Y. Wang, Synthesis of an efficient Pb adsorption nano-crystal under strong alkali hydrothermal environment using a gemini surfactant as directing agent, J. Chem. Soc. Pak., 41 (2019) 1034–1038.
[53] M. Eriksson, I. Lundstro, L. Ekedahl, A model of the Temkin isotherm behavior for hydrogen adsorption at Pd–SiO_2 interfaces, J. Appl. Phys., 82 (1997) 3143–3146.
[54] Z. Abdeen, S.G. Mohammad, Study of the adsorption efficiency of an eco-friendly carbohydrate polymer for contaminated aqueous solution by organophosphorus pesticide, Open J. Organ. Polym. Mater., 4 (2014) 16–28.
[55] A.S.A. Khan, Evaluation of thermodynamic parameters of cadmium adsorption on sand from Temkin adsorption isotherm, Turk. J. Chem., 36 (2012) 437–443.
[56] A. Ferguson, The Gibbs free energy of a chemical reaction system as a function of the extent of reaction and the prediction of spontaneity, J. Chem. Educ., 81 (2004) 606–611, doi: 10.1021/ed081p606.2.
[57] A. Kausar, H.N. Bhatti, G. Mackinnon, Equilibrium, kinetic and thermodynamic studies on the removal of U(VI) by low cost agricultural waste, Colloids Surf., B, 111 (2013) 124–133.
[58] L. Dehabadi, A.H. Karoyo, L.D. Wilson, Spectroscopic and thermodynamic study of biopolymer adsorption phenomena in heterogeneous solid–liquid Systems, ACS Omega, 3 (2018) 15370–15379.
[59] A.S. Bhatt, P.L. Sakaria, M. Vasudevan, Adsorption of an anionic dye from aqueous medium by organoclays: equilibrium modeling, kinetic and thermodynamic exploration, RSC Adv., 2 (2012) 8663–8671.
[60] S. Kustov, M.L. Corro, J. Pons, Entropy change and effect of magnetic field on martensitic transformation in a metamagnetic Ni–Co–Mn–In shape memory alloy, Appl. Phys. Lett., 94 (2009) 40–42.
[61] W.C. Zhang, S.T. Zhang, Z. Sun, First-principles study of molecular carbon dioxide adsorption in covalent organic framework-112, Sci. Adv. Mater., 11 (2019) 317–324.
[62] E. Virga, E. Spruijt, W.M.D. Vos, Wettability of amphoteric surfaces: the effect of pH and ionic strength on surface ionization and wetting, Langmuir, 4 (2018) 15174–15180.
[63] Y. Wang, Q. Lu, Dendrimer functionalized nanocrystalline cellulose for Cu(II) removal, Cellulose, 27 (2020) 2173–2187.
[64] X.Q. Pu, Y. Lu, Y. Lin, W.J. Jiang, X. Jiang, Utilization of industrial waste lithium-silicon-powder for the fabrication of novel nap zeolite for aqueous Cu(II) removal, J. Cleaner Prod., 265 (2020) 121822, doi: 10.1016/j.jclepro.2020.121822.
[65] S. Yang, J.C. Huo, Y.B. He, A. Wang, Adsorption kinetics, isotherms, and thermodynamics of Cr(III), Pb(II), and Cu(II) on porous hydroxyapatite nanoparticles, J. Nanosci. Nanotechnol., 18 (2018) 3484–3491.
[66] H. Merrikhpour, M. Jalali, Comparative and competitive adsorption of cadmium, copper, nickel, and lead ions by Iranian natural zeolite, Clean Technol. Environ., 15 (2013) 303–316.
[67] A.A. Mohammed, I.S. Samaka, Bentonite coated with magnetite Fe_3O_4 nanoparticles as a novel adsorbent for copper(II) ions removal from water/wastewater, Environ. Technol. Innovation, 10 (2018) 162–174.
[68] W.P. Putra, A. Kamari, S.N.M. Yusoff, C.F. Ishak, A. Mohamed, N. Hashim, I.M. Isa, Biosorption of Cu(II), Pb(II) and Zn(II) ions from aqueous solutions using selected waste materials: adsorption and characterisation studies, J. Encapsulation Adsorpt. Sci., 4 (2014) 25–35.
[69] M. Imamoglu, O. Tekir, Removal of copper(II) and lead(II) ions from aqueous solutions by adsorption on activated carbon from a new precursor hazelnut husks, Desalination, 228 (2008) 108–113.